Electronic supplementary information

Λ-Shaped donor-π-acceptor-π-donor molecule with AIEE and CIEE activity and sequential logic gate behaviour

Xiaofei Mei[a], Guixiu Wen[b], Jingwei Wang[b], Huimei Yao[b], Yan Zhao[b], Zhenghuan Lin[b]* and Qidan Ling[a,b]*

[a]*College of Chemistry and Chemical Engineering, Fujian Normal University, Fuzhou 350007, China.*

[b]*Fujian Key Laboratory of Polymer Materials, College of Materials Science and Engineering, Fuzhou 350007, Fujian, China.*

E-mail: zhlin@fjnu.edu.cn; qdling@fjnu.edu.cn

Measurements

Electronic spray ion (ESI) mass spectra were recorded on a TSQ Quantum Access MAX of Thermo Fisher Scientific. NMR spectra were measured in $CDCl_3$ on a Bruker Ascend 400 FT-NMR spectrometer; ^{1}H and ^{13}C chemicalshifts were quoted relative to the internal standard tetramethylsilane. Differential scanning calorimetry was done on a Perkin-Elmer DCS-7 instrument in the temperature range of 30–310 °C under flowing N_2 gas at a heating rate of 10 °C/min. UV-vis spectra were obtained on a Shimadzu UV-2600 spectrophotometer. The PL spectra were probed on a Shimadzu RF-5301PC fluorescence spectrophotometer. Melting points were measured by DSC analysis. The thermal annealing processes were carried out in an oven. All photographs were recorded on a Canon Powershot G7 digital camera under UV light (365 nm). Powder X-ray diffraction (PXRD) data were collected using an X'pert Pro diffractometer (Philips, USA) with Cu *Kα* radiation. Grazing incidence X-ray diffraction (GIXRD) data was collected using a SmartLab diffractometer (Rigaku, JP). The fluorescence lifetime and absolute Φ_F values of solution and solid were measured using an Edinburgh Instruments FLS920 Fluorescence Spectrometer with a 6-inch integrating sphere.

Materials

All of the reagents and solvents used in the experiment, were obtained from commercial suppliers and were used without further purification unless otherwise noted. N-methyl-3,4-dibromomaleimide and 4-(9-Carbazoly)phenyl boronic acid were synthesized according to the previously reported methods.[1,2] Thin layer chromatography was performed on MERCK Silica Gel 60 thick layer plates. Column chromatography was performed on Sorbent Technologies brand silica gel (40–63 mm, Standard grade).

Synthesis of (BCPMM)

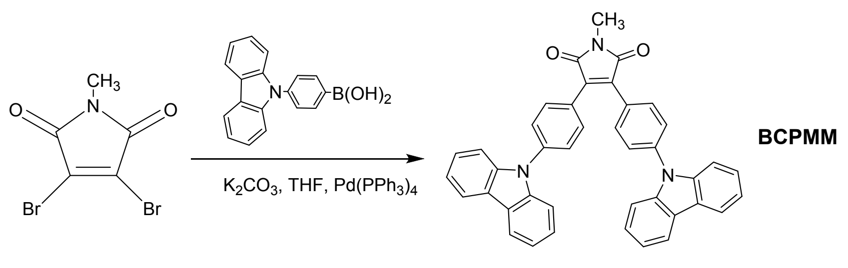

N-methyl-3,4-dibromomaleimide (0.64 g, 2.38 mmol) and 4-(9-Carbazoly)phenyl boronic acid (1.78 g, 6.19 mmol) were dissolved in 30 mL of THF. A 2M K_2CO_3 solution (10 mL) was added.

The reaction mixture was degassed with N_2 before adding 0.11 g of $Pd[P(C_6H_5)_3]_4$. The mixture was refluxed for 24 h before it was poured into water and extracted with dichloromethane. The organic layer was dried with Na_2SO_4, the solvent evaporated, and the crude product was purified by silica gel column chromatography with mixed solvent (dichloromethane: petroleum ether =1:1, v/v) to give yellow product (0.25 g, 18 %). ^{1}H NMR (*d*-$CDCl_3$, 400 MHz): δ 8.14 (d, J=8 Hz, 4H), 7.83 (d, J=8 Hz, 4H), 7.67 (d, J=12 Hz, 4H), 7.52 (d, J=8 Hz, 4H), 7.43 (t, J=8 Hz, 4H), 7.31 (t, J=8 Hz, 4H), 3.26 (s, 3H). ^{13}C NMR ($CDCl_3$, 100 MHz): δ 170.72, 140.23, 139.41, 135.60, 131.50, 127.17, 126.73, 126.14, 123.75, 120.49, 120.44, 109.82, 24.51. HRMS (ESI) m/z $[M+H]^+$ calcd 594.2176, found 594.2169.

X-ray Crystallography

The single crystals RC, YC1 and YC2 of BCPMM were mounted on a glass fiber for the X-ray diffraction analysis. Data sets were collected on a Rigaku AFC7R equipped with a graphite monochromated Mo-$K\alpha$ radiation (λ = 0.71073 Å) from a rotating anode generator at 293 K. Intensities were corrected for *LP* factors and empirical absorption using the ω scan technique. The structures were solved by direct methods and refined on F^2 with full matrix least-squares techniques using Siemens SHELXTL version 5 package of crystallographic software. All of the non-hydrogen atoms were refined anistropically. The positions of H atoms were generated geometrically (C-H bond fixed at 0.96 Å), assigned isotropic thermal parameters, and allowed to ride on their parent carbon atoms before the final cycle of refinement.

Reference

1. C. Marminon, A. Pierré, B. Pfeiffer, V. Pérez, S. Léonce, P. Renard and M. Prudhomme, *Bioorg. Med. Chem.*, 2003, **11**, 679-687.
2. L. Guo, K. F. Li, M. S. Wong and K. W. Cheah, *Chem. Commun.*, 2013, **49**, 3597-3599.

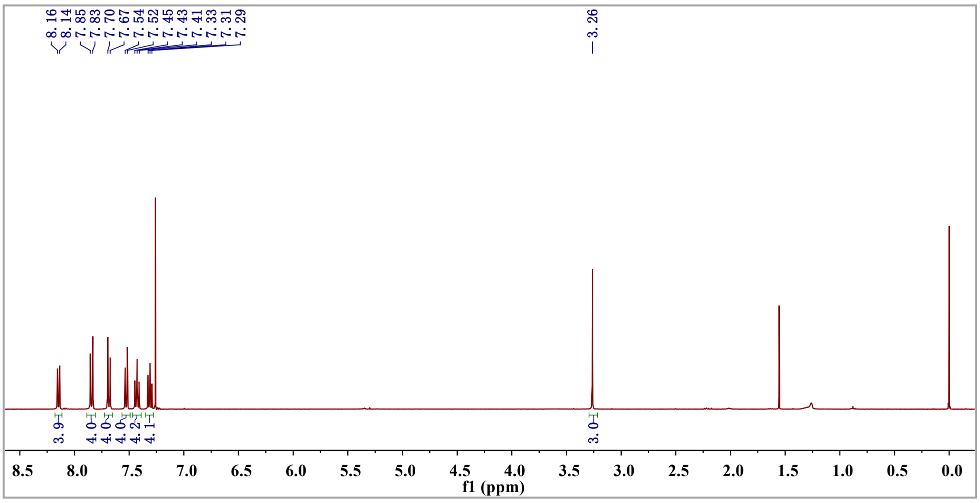

Fig. S1 ^{1}H NMR of BCPMM in *d*-$CDCl_3$.

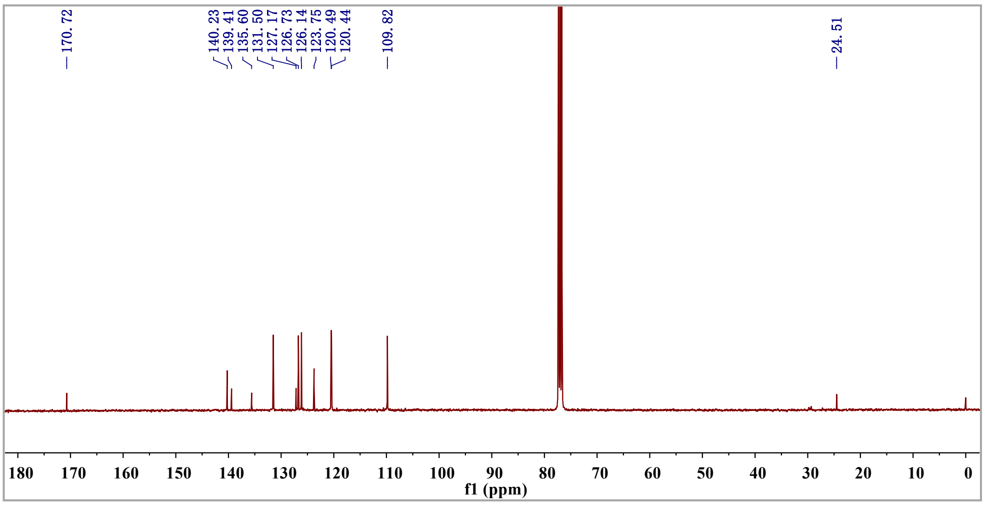

Fig. S2 ^{13}C NMR of BCPMM in *d*-$CDCl_3$.

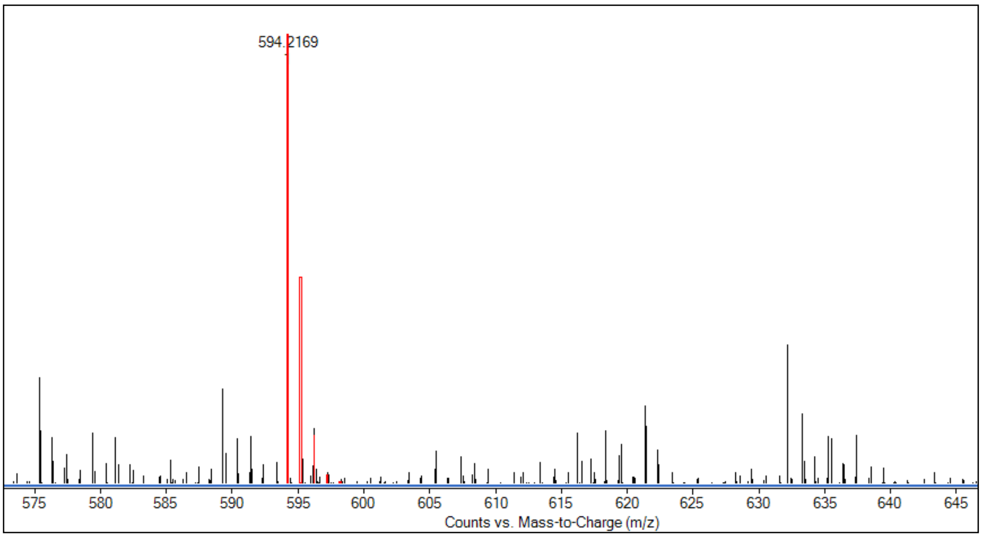

Fig. S3 High-resolution Mass of BCPMM.

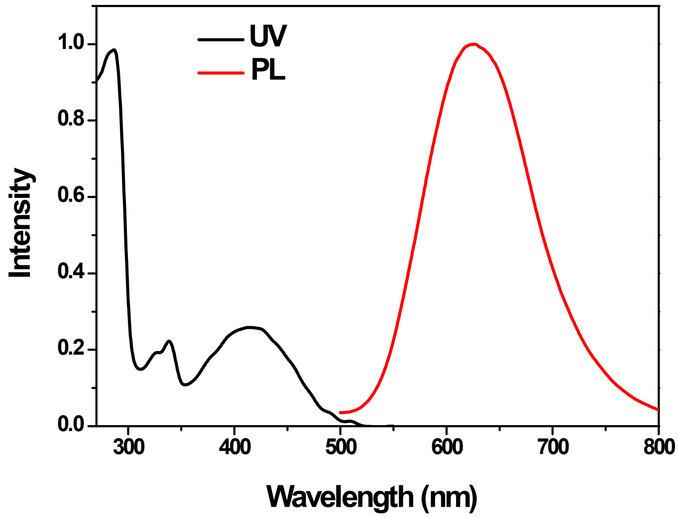

Fig. S4 Normalized absorption (UV) and fluorescence (PL) spectra of BCPMM in DCM solution.

Fig. S5 Digital photo of BCPMM in different solvents under UV lamp (365 nm). TOL= toluene; THF= tetrahydrofuran; DCM= dichloromethane; ACE= acetone; DMF= dimethyl formamide; ACN= acetonitrile.

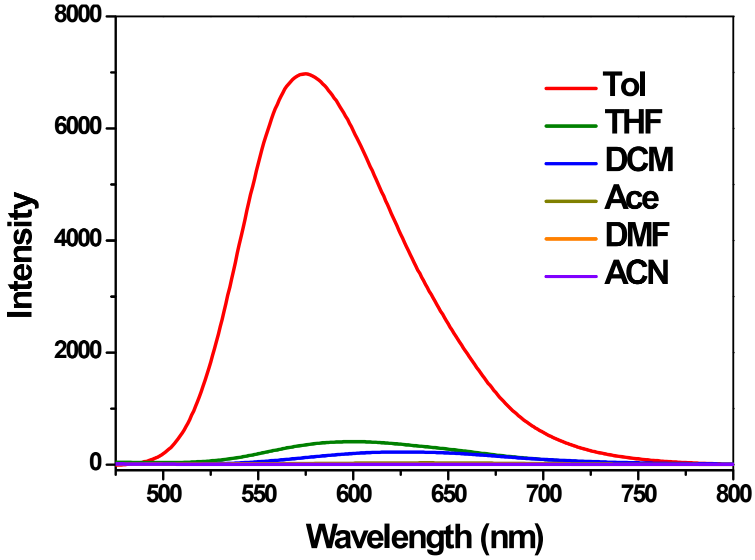

Fig. S6 Solvent effect on the emission spectra of BCPMM**.**

Table S1 Experimental data of photophysical properties of BCPMM in different solutions

Solvent	λ_{abs} (nm)	λ_{em} (nm)	Stokes shift (nm)	Φ_{em}
Tol	417	574	157	0.70
THF	409	601	192	0.15
DCM	415	626	211	0.04
Ace	397	643	246	0.01
DMF	401	649	248	0.001
ACN	396	649	253	＜0.001

Table S2 Experimental data of photophysical properties of BCPMM in different states.

States	λ_{em}, nm	Φ_F, %	τ_{av},[a] ns	k_r,[b] ns^{-1}	k_{nr},[c] ns^{-1}
Solution[d]	626	4	3.28	0.012	0.293
Aggregate[e]	604	35	8.45	0.057	0.063
Film	594	10	5.75	0.017	0.157
powder	566	38	7.70	0.049	0.081
YC1	553	72	7.3	0.099	0.038
YC2	557	80	9.37	0.085	0.021
RC	636	23	6.7	0.034	0.115

[a] Average lifetimes $\tau_{av} = \Sigma a_i \tau_i^2 / \Sigma a_i \tau_i$. [b]The radiative rate constant $k_r = \Phi_F / \tau_{av}$. [c]The non-radiative rate constant $k_{nr} = (1- \Phi_F) / \tau_{av}$. [d] DCM solution. [e]The aggregate in DCM-hexane (40 %: 60 %).

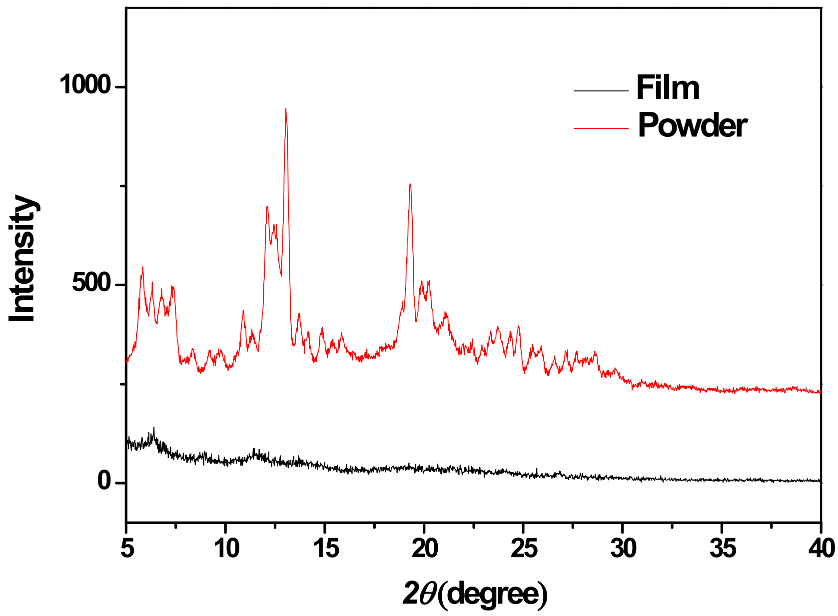

Fig. S7 XRD pattern of BCPMM in film and powder.

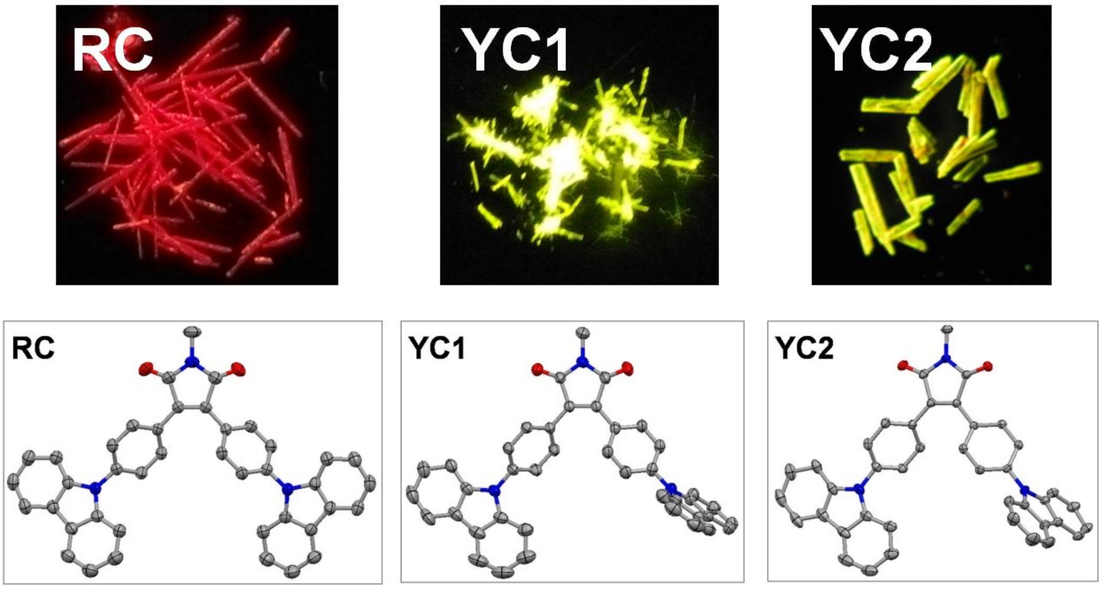

Fig. S8 (Upper) Digital photos of RC, YC1 and YC2 under UV lamp. (Bottom) Molecular structures of RC, YC1 and YC2 with the hydrogen atoms being omitted for calrity.

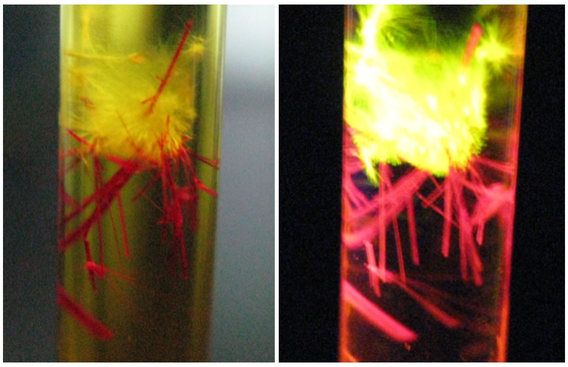

Fig. S9 Photos of RC and YC1 under daylight lamp (Left) and UV lamp (Right).

Table S3 Crystal data and structure refinement for RC, YC1 and YC2.

Crystal	RC	YC1	YC2
Formula	$C_{41}H_{27}N_3O_2$, $CHCl_3$ $C_{42}H_{28}Cl_3N_3O_2$	$C_{41}H_{27}N_3O_2$, $CHCl_3$ $C_{42}H_{28}Cl_3N_3O_2$	$C_{41}H_{27}N_3O_2$, $2(C_4H_8O)$ $C_{49}H_{43}N_3O_4$
Formula weight	713.02	713.02	737.86
Crystal system	orthorhombic	triclinic	monoclinic
Space group	Pbcn	P -1	C 1 2/c 1
a (Å)	23.9800(7)	9.0205(3)	26.2357(7)
b (Å)	17.7382(6)	10.9629(3)	15.5476(3)
c (Å)	8.0277(3)	17.9974(6)	19.4629(5)
α(deg)	90.00	78.085(3)	90.00
β(deg)	90.00	82.277(3)	107.126(3)
γ(deg)	90.00	80.414(3)	90.00
V ($Å^3$)	3414.7(2)	1707.87(9)	7586.9(3)
Z	4	2	8
$D_{calcd.}$(g/cm^3)	1.387	1.387	1.292
F(000)	1472	736	3120
R (int)	0.0412	0.0290	0.0213
GOF on F^2	1.034	1.147	1.019
R1[$I > 2\sigma(I)$]	0.0678	0.0429	0.0565
wR2[$I>2\sigma(I)$]	0.1743	0.1440	0.1499
R1 (all data)	0.1132	0.0501	0.0607
wR2(all data)	0.2073	0.1530	0.1536

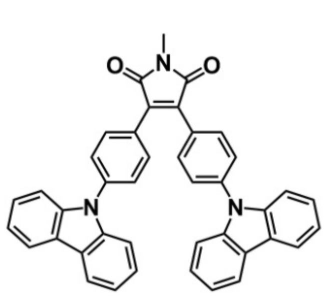

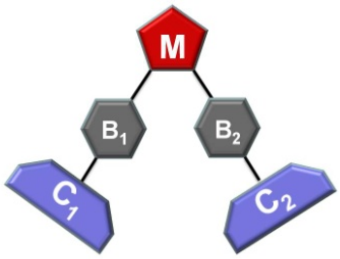

Table S4 The dihedral angle of maleimide ring with benzene and carbazole rings.

	MB_1	MB_2	MC_1	MC_2
Gas	36.8	37.3	88.7	88.2
RC	36.7	36.7	16.0	16.0
YC1	48.4	29.0	1.0	77.5
YC2	45.6	33.5	1.2	77.9

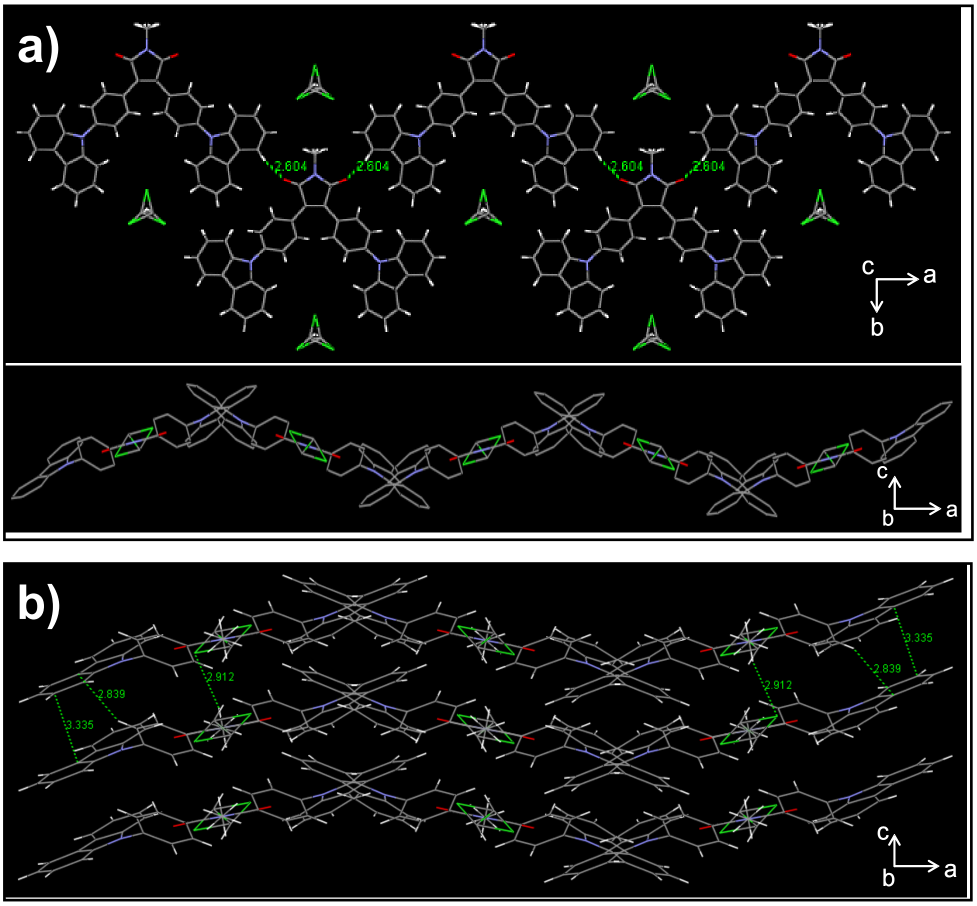

Fig. S10 The packing structures of RC. The hydrogen atoms in some pictures have been omitted for calrity.

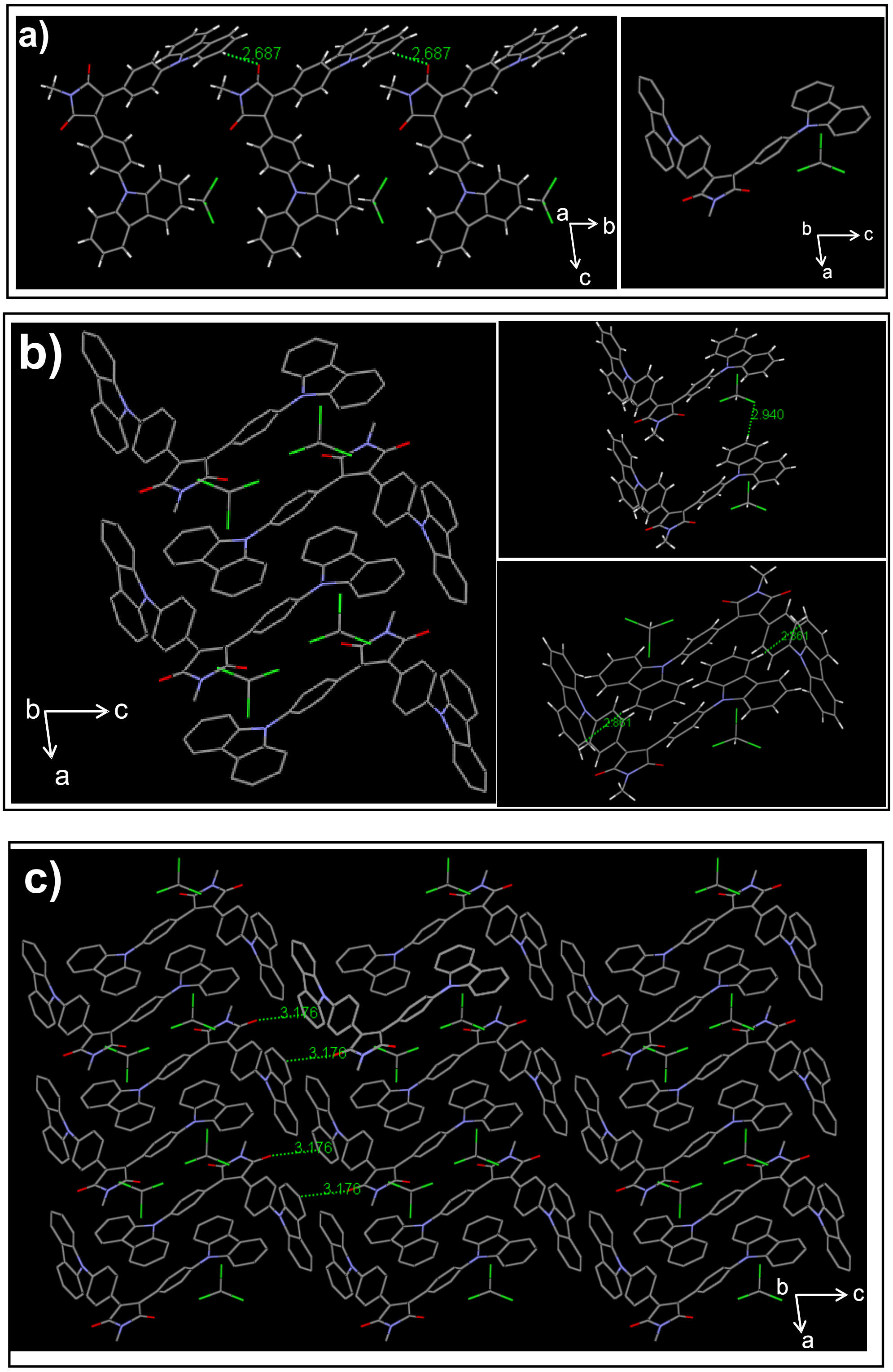

Fig. S11 The packing structures of YC1. The hydrogen atoms in some pictures have been omitted for calrity.

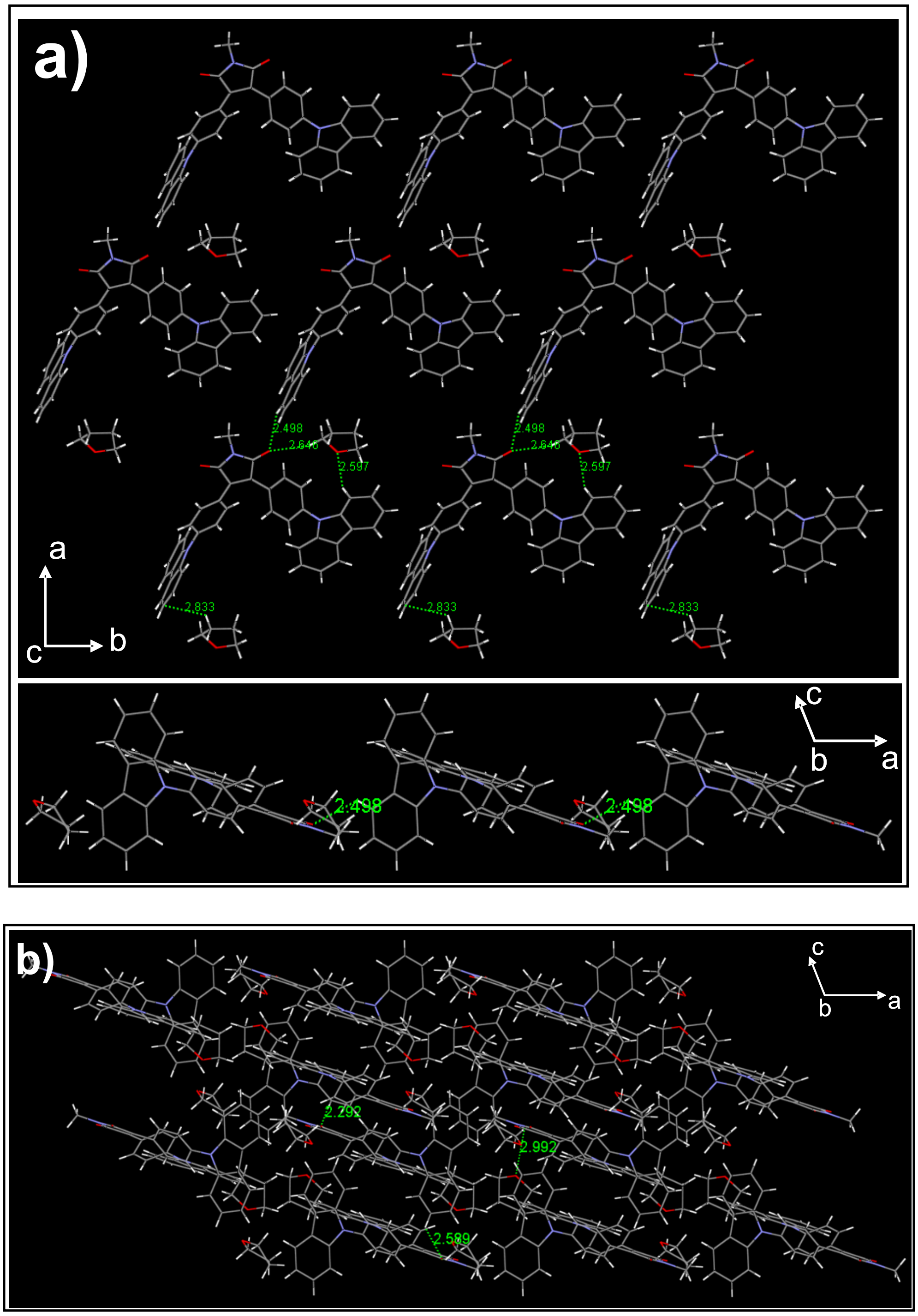

Fig. S12 The packing structures of YC2.

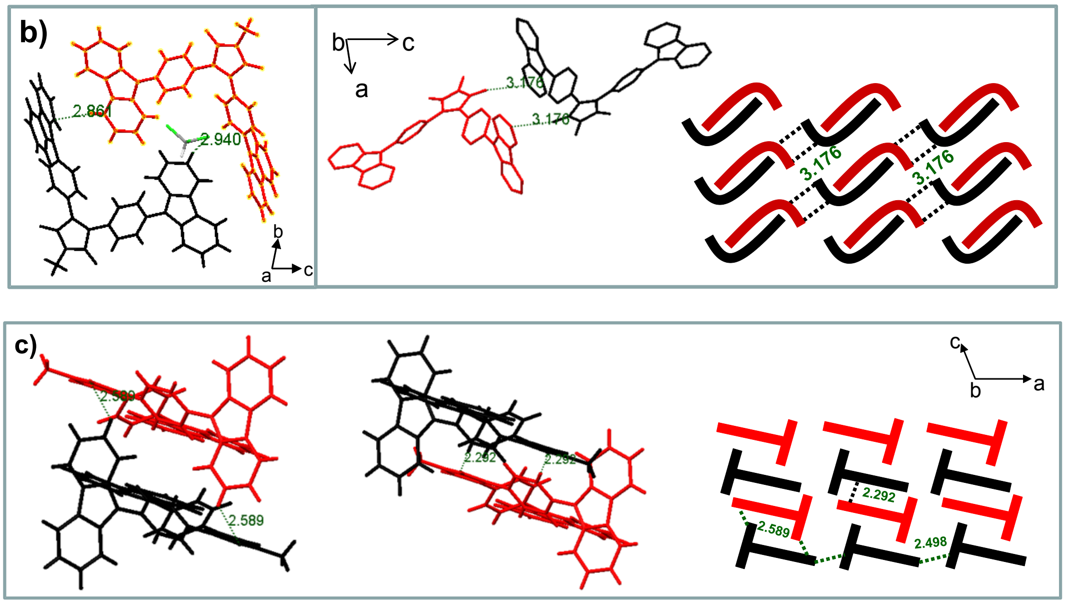

Fig. S13 An illustration of the packing structures of RC, YC1 and YC2.

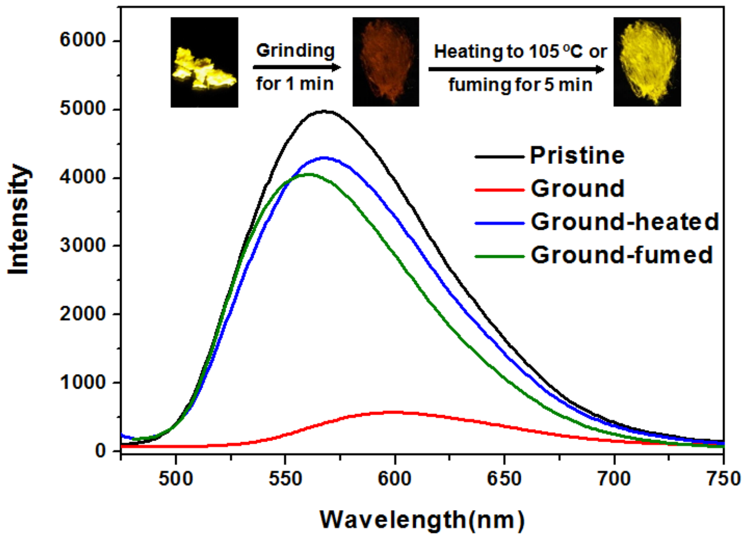

Fig. S14 The emission spectra of pristine, ground, ground-heated and ground-fumed powder.

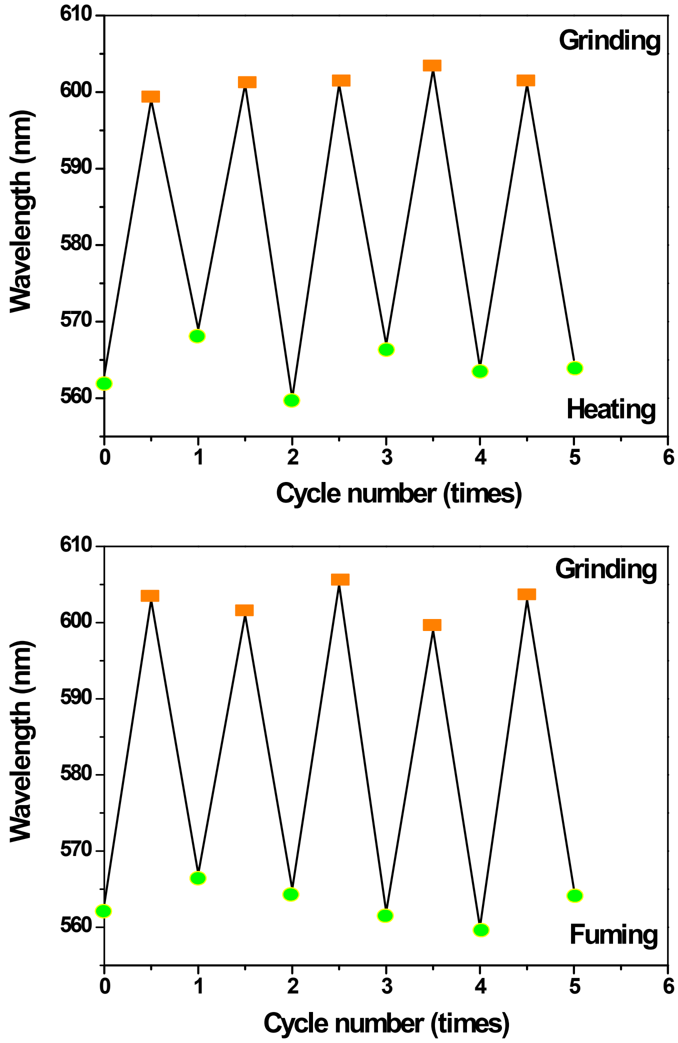

Fig. S15 Repeated switching between yellow and orange emission by heating-grinding cycles (Upper) and fuming-grinding cycles (Bottom).

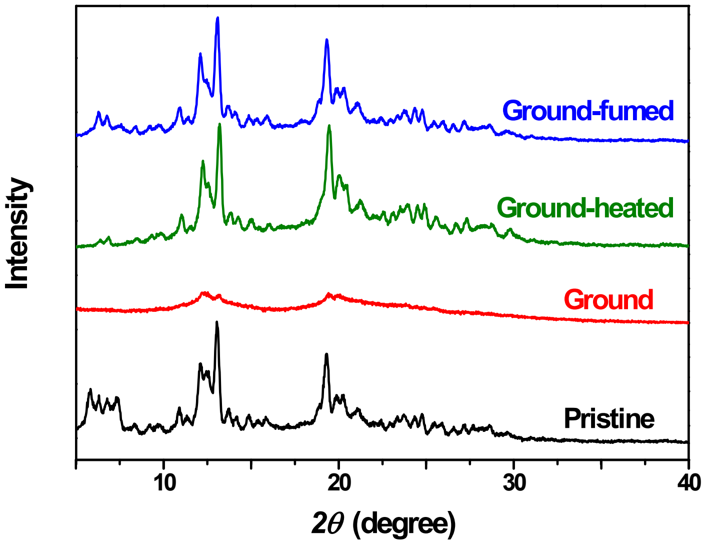

Fig. S16 The PXRD pattern of pristine, ground, ground-heated and ground-fumed powder.

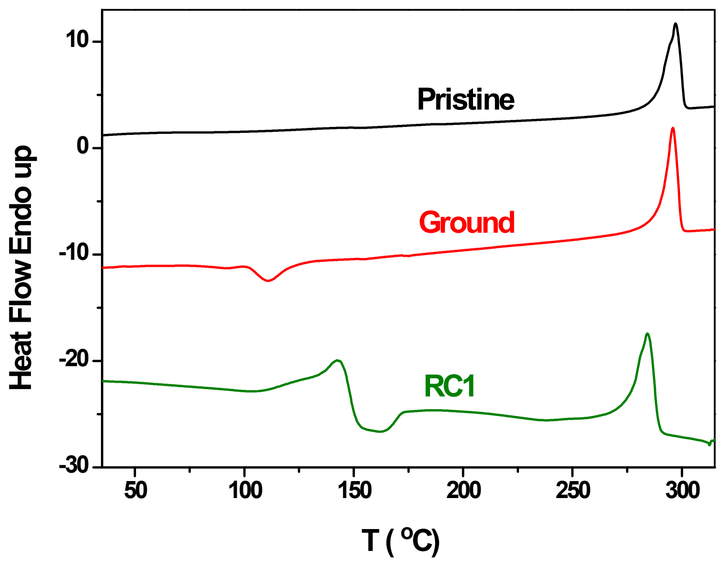

Fig. S17 The DSC plots of pristine and ground powder, and RC.

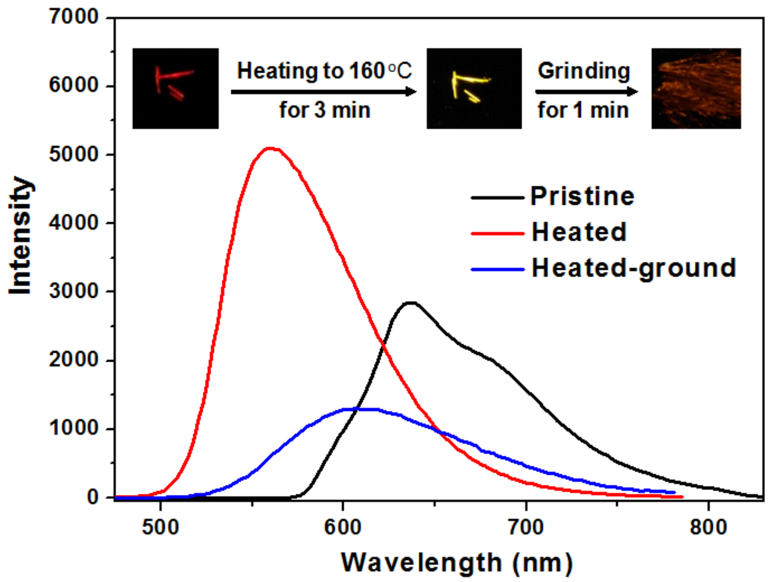

Fig. S18 The emission spectra of pristine, heated and heated-ground RC.

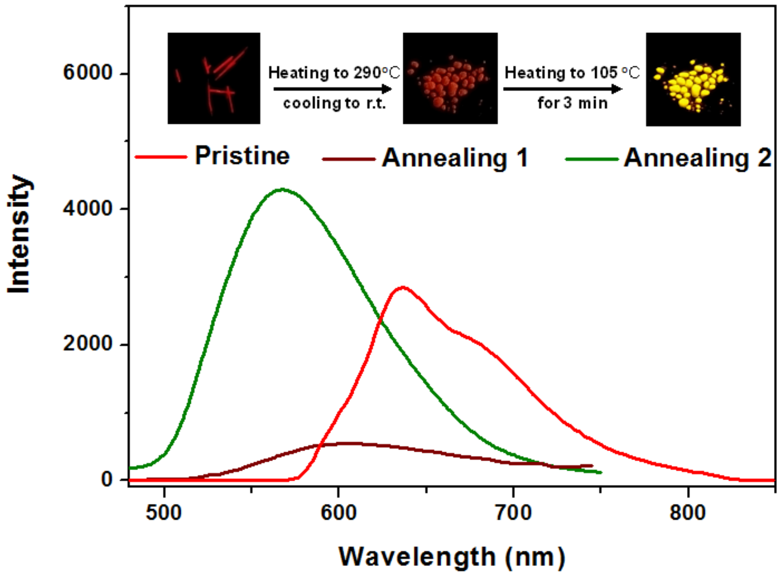

Fig. S19 The emission spectra of pristine and annealing RC.

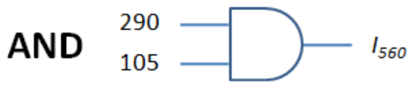

Entry	Input1	Input2	Output
	290℃	105℃	I_{560}
1	0	0	0 (6)
2	1	0	0 (316)
3	0	1	0 (15)
4	1	1	1 (4218)

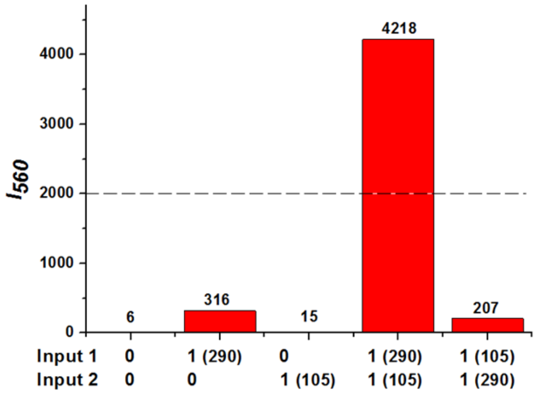

Fig. S20 True table of the AND logic gate and the fluorescence intensity at 560 nm (input i as the i input; threshold value of I =2000).

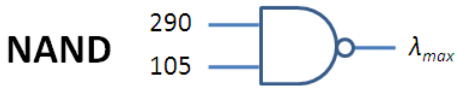

Entry	Input1	Input2	Output
	290℃	105℃	λ_{max}
1	0	0	1 (636)
2	1	0	1 (604)
3	0	1	1 (638)
4	1	1	0 (563)

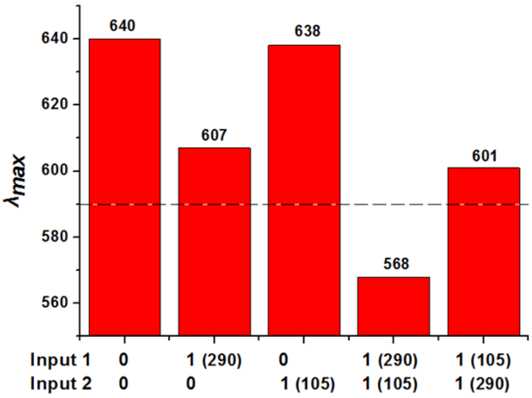

Fig. S21 True table of the NAND logic gate and the maximun emission wavelength (input i as the i input; threshold value of λ = 590 nm).

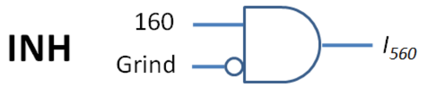

Entry	Input1	Input2	Output1
	160℃	grind	I_{560}
1	0	0	0 (10)
2	1	0	1 (5106)
3	0	1	0 (601)
4	1	1	0 (617)

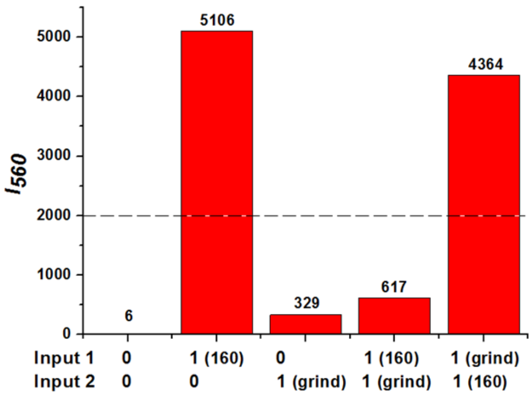

Fig. S22 True table of the INH logic gate and the fluorescence intensity at 560 nm (input i as the i input; threshold value of I =2000).

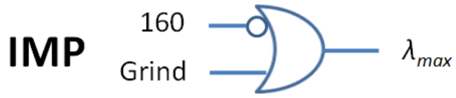

Entry	Input1	Input2	Output
	160℃	grind	λ_{max}
1	0	0	1 (640)
2	1	0	0 (560)
3	0	1	1 (638)
4	1	1	1 (608)

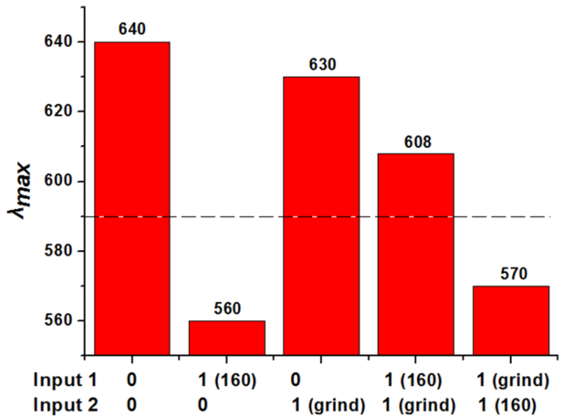

Fig. S23 True table of the IMP logic gate and the maximun emission wavelength (input i as the i input; threshold value of λ = 590 nm).

NOR

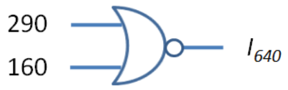

Entry	Input1	Input2	Output
	290℃	160℃	I_{640}
1	0	0	1 (2868)
2	1	0	0 (484)
3	0	1	0 (1378)
4	1	1	0 (1350)

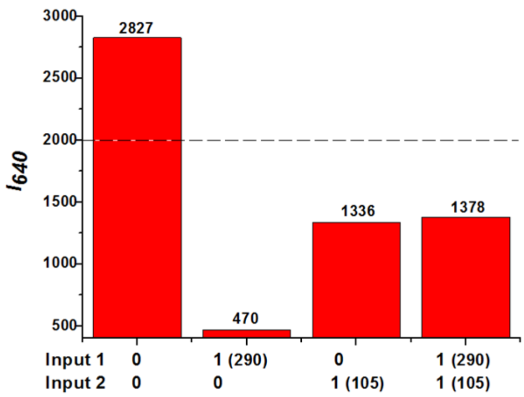

Fig. S24 True table of the NOR logic gate and the fluorescence intensity at 640 nm (input i as the i input; threshold value of I =2000).

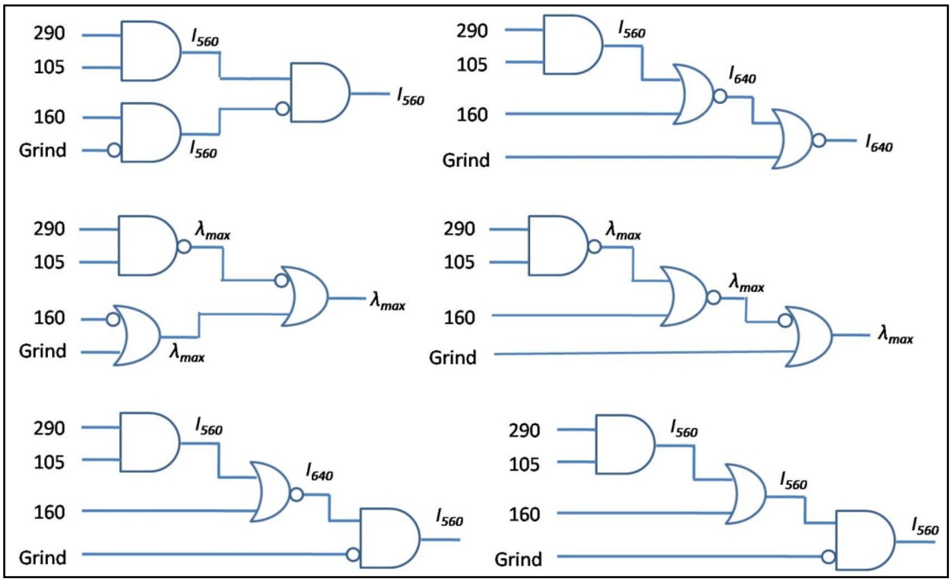

Fig. S25 Combinational logic operations with four sequential inputs (290 ℃, 105 ℃, 160 ℃ and grind) and three outputs (I_{560}, I_{640} or λ_{max}).

Table S5 True table of the combinational logic operations with four sequential inputs (290 ℃, 105 ℃, 160 ℃ and grind) and three outputs (I_{560}, I_{640} or λ_{max}).

Entry	Input1	Input2	Input3	Input4	Output1	Output2	Output3
	290℃	105℃	160	grind	I_{560}	I_{640}	λ_{max}
1	0	0	0	0	0 (6)	1 (2827)	1 (640)
2	1	0	0	0	0 (316)	0 (470)	1 (607)
3	0	1	0	0	0 (15)	1 (2826)	1 (638)
4	0	0	1	0	1 (5106)	0 (1336)	0 (560)
5	0	0	0	1	0 (329)	1 (2235)	1 (630)
6	1	1	0	0	1 (4218)	0 (1774)	0 (568)
7	1	0	1	0	1 (5096)	0 (1378)	0 (565)
8	1	0	0	1	0 (192)	0 (250)	1 (601)
9	0	1	1	0	1 (5308)	0 (1347)	0 (560)
10	0	1	0	1	0 (329)	1 (2235)	1 (630)
11	0	0	1	1	0 (617)	0 (1072)	1 (608)
12	1	1	1	0	1 (4227)	0 (1778)	0 (563)
13	1	1	0	1	0 (253)	0 (308)	1 (599)
14	1	0	1	1	0 (292)	0 (386)	1 (602)
15	0	1	1	1	0 (212)	0 (316)	1 (603)
16	1	1	1	1	0 (383)	0 (726)	1 (607)

Table S6 True table of the combinational logic operations with four sequential inputs (290 ℃, 160 ℃, grind and 105 ℃) and two outputs (I_{560}, I_{640}).

Entry	Input1	Input2	Input3	Input4	Output1	Output2
	290℃	160℃	grind	105℃	I_{560}	I_{640}
1	0	0	0	0	0 (6)	1 (2827)
2	1	0	0	0	0 (316)	0 (470)
3	0	1	0	0	1 (5106)	0 (1336)
4	0	0	1	0	0 (329)	1 (2235)
5	0	0	0	1	0 (15)	1 (2826)
6	1	1	0	0	1 (5096)	0 (1378)
7	1	0	1	0	0 (192)	0 (250)
8	1	0	0	1	1 (4218)	0 (1774)
9	0	1	1	0	0 (617)	0 (1072)
10	0	1	0	1	1 (5156)	0 (1348)
11	0	0	1	1	0 (504)	1 (2239)
12	1	1	1	0	0 (292)	0 (386)
13	1	1	0	1	1 (5125)	0 (1402)
14	1	0	1	1	1 (4227)	0 (1778)
15	0	1	1	1	1 (4374)	0 (1503)
16	1	1	1	1	1 (4368)	0 (1515)

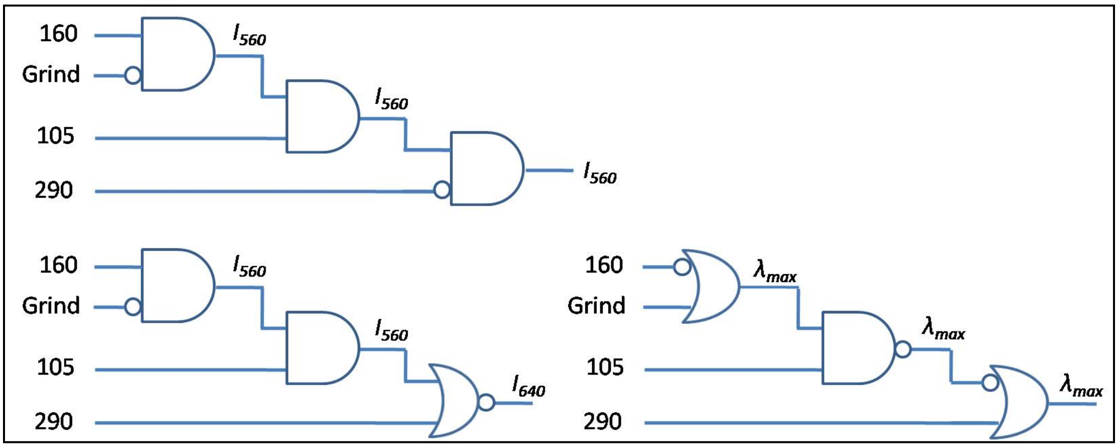

Fig. S26 Combinational logic operations with four sequential inputs (160 ℃, grind, 105 ℃ and 290 ℃) and three outputs (I_{560}, I_{640} or λ_{max}).

Table S7 True table of the combinational logic operations with four sequential inputs (160 ℃, grind, 105 ℃ and 290 ℃) andthree outputs (I_{560}, I_{640} or λ_{max}).

Entry	Input1	Input2	Input3	Input4	Output1	Output2	Output3
	160℃	grind	105℃	290	I_{560}	I_{640}	λ_{max}
1	0	0	0	0	0 (6)	1 (2827)	1 (640)
2	1	0	0	0	1 (5106)	0 (1336)	0 (560)
3	0	1	0	0	0 (329)	1 (2235)	1 (630)
4	0	0	1	0	0 (15)	1 (2826)	1 (638)
5	0	0	0	1	0 (316)	0 (470)	1 (607)
6	1	1	0	0	0 (617)	0 (1072)	1 (608)
7	1	0	1	0	1 (5156)	0 (1348)	0 (559)
8	1	0	0	1	0 (457)	0 (505)	1 (602)
9	0	1	1	0	0 (504)	1 (2239)	1 (628)
10	0	1	0	1	0 (285)	0 (480)	1 (602)
11	0	0	1	1	0 (207)	0 (457)	1 (601)
12	1	1	1	0	1 (4374)	0 (1503)	0 (565)
13	1	1	0	1	0 (253)	0 (308)	1 (599)
14	1	0	1	1	0 (276)	0 (350)	1 (601)
15	0	1	1	1	0 (180)	0 (296)	1 (603)
16	1	1	1	1	0 (213)	0 (262)	1 (597)